Compression of filled, open-cell, 3D-printed Kelvin lattices

J. Carlsson*, A. Kuswoyo*, A. Shaikeea and N. A. Fleck**

Cambridge University Engineering Dept., Trumpington St., Cambridge, CB2 1PZ, UK

*joint first author, ** corresponding author

30 October 2023

Abstract

The sensitivity of compressive strength of a polymeric Kelvin lattice to the presence of an epoxy core has been investigated both experimentally and numerically. Crush bands develop in the empty lattice, with large oscillations in load due to geometric softening and the sequential fracture of successive layers of struts. In contrast, the epoxy core has a sufficiently high modulus and strength that outward lateral flow of the epoxy through the open-cell lattice is negligible: the boundary layer, wherein migration of epoxy occurs through the lattice, extends less than one cell size from the surface of the specimen. The epoxy core supports the struts and stabilises the bulk macroscopic response against crush band formation. Finite element analysis of periodic unit cells show that the presence of an almost incompressible epoxy core changes the deformation mode of the lattice from one that is close to uniaxial straining to an isochoric mode. However, both the compressible collapse mode of the empty lattice and the isochoric deformation mode of the filled lattice are bending-dominated. At finite strain, the observed macroscopic strength of the filled lattice is degraded by bending failure of the struts and by tensile cracking of the adjacent core; the failure location is at a particular subset of the nodes of the lattice. Microcrack coalescence leads to the formation of a series of vertical fissures in the specimen.

Keywords: Kelvin lattice, multi-phase cellular solid, additive manufacturing, crush bands

1. Introduction

The Kelvin cell is an excellent idealized representation of natural and artificial foams, see Fig. 1(a) (Gibson and Ashby, 1997; Simone and Gibson, 1998; Ashby et al., 2000; Chen et al., 2018). Lord Kelvin (1887) conjectured that a packing of tetrakaidecahedra, based on the truncated octahedron but with slightly curved faces, is the most efficient packing arrangement to achieve the minimum surface energy per unit volume. More than one century later, Weaire and Phelan (1994) discovered a slightly more efficient packing that comprises two irregular pentagonal dodecahedra and six tetrakaidecahedra; this is the so-called Weaire-Phelan packing. The present study makes use of the simpler Kelvin lattice as the difference in mechanical responses between the Kelvin and Weaire-Phelan packings is rather small, as reviewed by Chen et al (2018). Also, the Kelvin packing is commonly observed, as mentioned above.

Typically, as-manufactured open or closed cell lattices contain a compressible gas such as air, and the contribution of this core to the macroscopic response is negligible. However, there is scope to fill the lattice with a second phase to enhance multifunctionality such as improved (or reduced) heat exchange or modify electrical conductivity. The lattice can serve as a 3D reinforcement of the interpenetrating phase: it can elevate macroscopic mechanical properties such as compressive strength, see for example Tzortzinis et al. (2022). The existing literature is almost silent on this topic despite the fact that the manufacture of a filled open-cell lattice is straightforward: open-celled lattices can be filled by dipping them in a liquid and then allowing the liquid core to harden or solidify. The filling of a closed cell lattice is more problematic, but can be achieved by emerging methods of additive manufacture and by biological growth processes. For example, adipose tissue contains closed cells (adipocytes) that are filled with globules of lipid with the properties of a low viscosity oil, see for example Comley and Fleck (1994). It is recognised that a foams and lattices are useful for light weighting applications, and for energy absorption applications particularly in impact and blast (Tagarielli et al. 2007; McShane et al. 2006). The addition of a core adds weight, and so it is important to determine the degree to which a core can give structural advantage.

First, a note on notation. The Kelvin unit cell is commonly referred to in the literature as the Kelvin foam. Historically, the term ‘foam’ refers to a random, open or closed cell 3D topology that has been manufactured from the liquid state and approximates a minimum energy configuration, with a nodal connectivity of typically 3-4 struts per node. However, foams are

usually random in microstructure whereas lattices have a periodic, crystallographic topology. Hence, we shall refer to the Kelvin unit cell as the Kelvin lattice.

1.1 The compressive response of an empty Kelvin lattice

The compressive strength of an open or closed cell Kelvin lattice is dictated either by elastic buckling or by yield of the cell walls. Elastic buckling dominates when the lattice possesses a sufficiently low relative density $\bar{\rho}$ in relation to yield strain of the cell wall material. Gong et al. (2005) have performed an in-depth elastic bifurcation analysis of an open-cell Kelvin lattice using Bloch wave analysis and general macroscopic loading. They identified a rich variety of buckling modes. For some directions of macroscopic loading the critical modes have long wavelengths and result in an unstable postbuckling behaviour. Under other loading states, the modes are of short wavelength and the postbuckling response is stable.

In the present study, we shall focus on lattices that compress in an elastic-plastic manner. Gibson and Ashby (1997) have made analytical predictions of the macroscopic modulus and strength of empty lattices such as the Kelvin lattice: they find that the mechanical properties of the open-cell lattice are governed by elasto-plastic bending of the cell walls whereas the macroscopic response of the closed-cell lattice involves bending of the cell edges and stretching of the cell faces. Consequently, the compressive strength of an open-cell lattice scales with relative density $\bar{\rho}$ to the power of 3/2 whereas the strength of a closed-cell lattice with pronounced cell faces scales linearly with relative density. Uniaxial compression of open or closed cell lattices commonly leads to the formation of crush bands and to an oscillating macroscopic stress versus strain response (Jang et al. 2010; Jang and Kyriakides 2009a, 2009b; Chen et al. 2018; Carlsson et al. 2023).

Jang et al. (2009b, 2010) and Park et al (2022) performed finite element (FE) simulations of the macroscopic compressive response of an open-cell Kelvin lattice. They predicted that a unit cell and a finite specimen give almost identical macroscopic responses provided the finite specimen contains more than 3 unit cells in each direction. Mild softening occurs in the periodic unit cell, and finite specimens give rise to inclined crush bands. It is evident from the studies of Jang et al. (2009b, 2010) that the unit cell representation is adequate for the early stages of the elastic-plastic response. We further note that Jang et al. (2009b, 2010) considered metallic lattices of sufficient ductility that strut failure did not arise. In contrast, in the present study,

polymeric lattices were manufactured and tested, and it will be shown that the macroscopic response is degraded by strut failure. Localisation of buckling from an initial periodic mode into a crush band is an example of the general phenomenon of the localisation of buckling patterns as explored by Tvergaard and Needleman (1980).

Instabilities do not always arise in the elasto-plastic compressive response of an empty lattice: the collapse mode can be stable by choosing a cell wall material of sufficiently high strain hardening capacity. For example, Wang et al. (2023) manufactured open-cell Kelvin lattices by selective laser melting (SLM) of 316L stainless steel powder. The strain hardening rate of this stainless steel is sufficiently high to prevent localization by cell wall crushing, and a stable compressive response was observed.

1.2 The compressive response of a filled Kelvin lattice

There are few studies in the literature on the effect of a core reinforcement upon the macroscopic compressive response of a Kelvin lattice. Wang et al. (2023) manufactured an open cell Kelvin lattice from 316L stainless steel and added a polystyrene lattice core. They observed a negligible increase in the compressive strength, and confirmed this by finite element simulations. This is not surprising given the high compressibility and low strength of polystyrene foam in relation to that of the empty stainless steel lattice. In present study, the core material (epoxy) is almost incompressible and its uniaxial strength is comparable to that of the empty lattice: interaction effects between core and lattice are anticipated.

The addition of a core to an open or closed cell lattice will reinforce the response, but the details are largely unknown. Recently, experimental and numerical studies have been performed on the effect of an inviscid, incompressible core upon the macroscopic response of a 2D honeycomb, which is the 2D analogue of a closed cell 3D lattice (Tankasala et al. 2021; Carlsson et al. 2022; Shalchy et al. 2022). These studies reveal that cavitation of the core by debonding from the lattice or by voiding has a major effect upon collapse response of the filled lattice. When cavitation is prevented by the presence of a sufficiently high macroscopic pressure, the compressive response of the filled honeycomb displays a structural instability in the form of inclined shear banding that involves softening in shear at constant volume. Carlsson et al. (2022) noted an extreme sensitivity of this instability to the geometry of the honeycomb, such as the inclination of the cell walls.

Carlsson et al. (2023) have recently performed finite element predictions of the macroscopic compressive response of a *closed-cell* Kelvin lattice in both an empty state and filled by an inviscid, incompressible fluid. The cell walls of the Kelvin lattice were treated as elastic, ideally plastic. For the empty closed-cell lattice with negligible Plateau borders, the macroscopic modulus and strength scale almost linearly with the relative density of the lattice due to stretching of the cell walls. The addition of an inviscid, incompressible core has a minor effect upon the macroscopic modulus and yield strength but has a major stabilizing influence upon the macroscopic post-yield response. An aim of the present study is to determine the degree of reinforcement of an *open-cell* Kelvin lattice due to the addition of an incompressible core of finite modulus and strength. This is the practical case, as it is straightforward to manufacture filled, open-cell Kelvin lattices. We note in passing the obvious result that the filling of open-cell lattice by an inviscid fluid has no effect upon its macroscopic response as the core simply leaks out of the lattice. Thus, the following questions give focus to our study:

1. Does the addition of a core change the dependence of macroscopic modulus and strength upon relative density of the lattice?

2. Does the addition of a core stabilize the post-yield response and eliminate the formation of crush bands?

The scope of the present study is to manufacture and then perform compression tests on polymeric, open cell Kelvin lattices in the empty and filled states. Thereby, the effect of the core, and of the relative density of the Kelvin lattice upon the collapse response is explored both experimentally and by finite element simulations.

2. Materials and Method

2.1 Manufacture of specimens

The empty, open-cell Kelvin lattice

Cube-shaped polymeric specimens of open-cell Kelvin lattice were manufactured by stereolithography[1] (SLA). A proprietary photosensitive 'grey resin' (Grey V4, Formlabs[2]) was used: the grey resin is a photosensitive liquid containing methacrylate polymer and

[1] Formlabs 3D SLA printer model Form 3
[2] https://formlabs.com

photoinitiator that solidifies when exposed to the 405 nm light. SLA printing of the grey resin was performed using a layer-by-layer thickness of 50 microns, and immediately after printing the specimens were washed in isopropyl alcohol for 10 minutes and then UV cured at 60°C for 60 minutes. All specimens were stored in a darkened cupboard to prevent over-curing and were tested within a month of printing.

The geometry of the Kelvin cell specimens is shown in Fig. 1. The unit cell dimension L and strut diameter d were defined in Standard Tessellation Language (STL) files using the software package nTopology[3]. To create the geometry, the Kelvin lattice was defined by a list of nodal points and nodal connectivity. Struts, of diameter d = 0.6 mm were then generated, and the unit cell size L was in the range 3.63 mm to 6.60 mm in order to give a relative density $\bar{\rho}$ of 0.04 to 0.14. The measured densities were close to the design values; this was verified by X-ray tomography. Small Plateau borders of root radius R =0.1 mm were added in order to reduce stress concentrations within the lattice. This small modification to geometry is shown in Fig. A1 of the Appendix; it is also reported in the Appendix via a series of finite element simulations that the effect of Plateau borders upon the compressive response of the empty and filled lattice is negligible. An additional layer of unit cells (of enlarged strut diameter equal to 1.2 mm) was added followed by solid platens of thickness of 4 mm, see Fig. 1(b). The additional layer of thickened struts and the fully dense top and bottom plates ensured uniform loading of the lattice upon compressing between the platens of the test machine. The as-manufactured lattices contained 9x9x9 unit cells to give a macroscopic response that is independent of the number of unit cells[4].

The filled Kelvin lattice

The filled lattice specimens were manufactured as follows. First, an empty lattice specimen was placed into a silicone rubber mould of dimension equal to that of the specimen. Then, the cavity was filled with filled flexible epoxy resin EF80 (Easy Composites Ltd, UK[5]) using a resin-to-hardener mix ratio of 100:145 (parts by weight). The resin was allowed to cure fully over 7 days before the composite specimen was removed from the mould.

[3] https://ntop.com
[4] The experimental and numerical study of Wang et al (2023) reveals that the compressive response of an open cell Kelvin lattice comprising n x n x n unit cells is insensitive to the value of n in the range 3 to 5.
[5] https://easycomposites.co.uk

Specimens made from grey resin and EF80 epoxy

Tensile, dogbone specimens of diameter 0.6 mm and gauge length 2 mm were made from the grey resin. The diameter of the specimens was chosen to match that of the struts in order to ensure that the degree of cure in the tensile specimens matches that in the filled Kelvin lattices. Three sets of grey resin struts were printed, such that the strut orientation relative to the print direction was 0°, 45°, and 90°; the aim was to determine the sensitivity of uniaxial tensile response of the cured strut resin to both the direction of printing relative to the loading direction.

Tensile dogbone specimens were also prepared from cured EF80 epoxy, with a square cross-section 6 mm x 6 mm and gauge length of 25 mm. The extension of the gauge length in the tensile tests was recorded by video for the cured strut resin and by a laser extensometer for the EF80 epoxy. Additionally, cube-shaped specimens of EF80 and of side length 20mm were manufactured in order to measure the compressive response.

2.2 Mechanical Tests

Compression tests were performed on both empty and filled regular Kelvin lattices in order to determine the sensitivity of compressive response to the presence of a core. The cuboid-shaped specimens were compressed at a nominal strain rate of 10^{-3} s^{-1} in a screw-driven test machine, and a laser extensometer was used to measure the gauge section extension.

The uniaxial tensile response of the as-cured grey resin in strut form was measured by performing tensile tests on the dogbone-shaped struts. The sensitivity of response to (i) the direction of printing relative to the loading direction, and (ii) to the effect of strain rate in the range 10^{-4} s^{-1} to 10^{-2} s^{-1} was determined. Tensile and compressive tests were performed on the cured EF80 by making use of the dogbone and cube-shaped specimens, respectively.

3. Experimental Results

3.1 Material Properties

The tensile nominal stress versus nominal strain responses of the grey resin and EF80 are given in Fig. 2. The EF80 behaves in a hyperelastic manner, with a response that is almost independent of strain rate in the range 10^{-4} s^{-1} to 10^{-2} s^{-1} (not shown), and is able to stretch to a large nominal strain on the order of 0.8 before tearing. Repeat tests were performed (not shown for the sake of clarity) and give negligible scatter in response. The EF80 has a Young's modulus equal to 4.7 MPa and is treated as a single parameter neo-Hookean solid in the finite element simulations that are reported below. The compressive nominal stress versus nominal strain response of the EF80 is included in Fig. 2(a). The initial, small strain response is identical to that exhibited in the tensile tests. At larger strain levels, the nominal compressive response is stiffer than the corresponding tensile response, as expected.

Tensile tests on the grey resin reveal that it behaves as a rate dependent, elastic-plastic solid, with negligible strain hardening, see Fig. 2(b) for 3 selected strain rates of $\dot{\varepsilon}$=10^{-4} s^{-1}, 10^{-3} s^{-1} and 10^{-2} s^{-1}. Three identical tests at each imposed strain rate reveal little scatter in material response. The tensile response shown in Fig. 2(b) is for a build direction of the SLA printing process that is inclined at 45^{o} to the axial direction: this is the most common orientation of struts in the Kelvin cell. The fracture surface of the tensile specimens reported in Fig. 2(b) are planar with no sign of necking; fracture initiates from randomly located surface or internal defects, and the unit normal to the fracture surface is aligned with the loading direction. This observation suggests that the degree of anisotropy in tensile response of the specimens is negligible. In order to confirm this, additional tests were performed with the build direction co-axial with the loading direction of the tensile tests, and with the build-direction orthogonal to the loading direction. The results are shown in Fig. A2 of Appendix A, and confirm that the response is almost isotropic; in consistent fashion, the failure surface in each test is always normal to the loading direction.

Based on the results of Fig. 2(b) and Fig. A2, the grey resin was assumed to behave as an elastic- power law creeping solid with a Young's modulus E =1.58 GPa and Poisson ratio ν = 0.35. The true creep rate $\dot{\varepsilon}$ is related to a true uniaxial stress σ in a power law manner such that

$$\frac{\dot{\varepsilon}}{\dot{\varepsilon}_0} = \left(\frac{\sigma}{\sigma_o}\right)^m \qquad (1)$$

where the reference flow strength is σ_0 = 34 MPa at a reference value of strain rate chosen to be $\dot{\varepsilon}_0 = 10^{-3}$ s^{-1}; the strain rate exponent is $m = 9.15$. The quality of fit of this power law creep relation is assessed by comparing directly the flow strength from (1) with the observed plateau value of stress. Thus, at a strain rate of 10^{-4} s^{-1}, 10^{-3} s^{-1} and 10^{-2} s^{-1}, respectively, the measured average value of flow strength reads 30 MPa, 35 MPa and 45 MPa, while the formula (1) gives 27 MPa, 34 MPa and 44 MPa.

3.2 Compression response of the empty and filled lattices

Compression tests were performed on both the empty and filled lattices at a nominal strain rate of 10^{-3} s^{-1}, see Fig. 3 for representative measurements at 3 values of relative density. Scatter from test to test is only mild, as evidenced by a complete set of data assembled in Fig. A3. The empty lattice has an initial elastic response, followed by plastic collapse that involves the formation of a series of crush bands, with an oscillation in load associated with each successive crush band. The pronounced softening is associated with fracture of individual struts[6]. In contrast, a stable response is evident for the filled lattices, with no crush band formation and no oscillation in load.

In-situ compression tests in a X-ray CT machine reveal that struts in the filled lattice break at nodes in a progressive and distributed manner within the specimen, as shown in Fig. 4. A loading rig was devised so that both the axial load and displacement in a compression test could be measured inside the CT machine, and 3D tomographs could be obtained with the specimen under load. Specifically, a filled lattice (lattice relative density of 0.09 and manufactured from a specimen consisting of 4x4x9 unit cells) was compressed, and 3D scans of the whole specimen were obtained at an axial strain of 0.1, 0.2 and 0.3. The 3D scans were post-processed in order to obtain an image of the vertical mid-plane of the specimen, and the resolution (100 μm) was adequate to resolve progressive cracking of the struts and adjacent matrix. At a compressive strain of 0.1 vertical cracks are present in approximately 10% of the top and bottom nodes that exist in a diamond configuration, see Fig. 4. With increased compressive straining, cracks form in additional nodes of diamond configuration, and these vertical cracks extend into the adjacent matrix. Note that axial compression in the struts is balanced by tension in the matrix in the *y*- direction orthogonal to the macroscopic loading direction *z*, as shown in

[6] Jang and Kyriakides (2009a; 2009b) found only mild oscillations in the compressive response both experimentally and by simulation for the case of an aluminum alloy of high ductility.

Fig. 4, thereby driving crack extension. The presence of the cracks in the struts and matrix reduces the macroscopic tangent modulus of the compressive response of the filled specimen, as evidenced by the comparison of Fig. 3(b) of finite element prediction (no cracks present) to experiment (cracks present). Full details of the finite element simulations are given below.

It is instructive to plot in Fig. 5 the measured strength of the filled and empty lattices at a fixed value of nominal strain of ε_n = 0.08 which is close to the peak strength of the empty lattice and close to the knee of the stress versus strain curve of the filled lattices. The log-log plot of strength versus relative density is of slope 2 for the empty lattice and is of much reduced slope for the filled lattice, see Fig. 5. The high slope for the macroscopic strength of the empty lattice is consistent with a bending mode of elastic deformation.

The uniaxial strength of the EF80 epoxy at a nominal strain of $\varepsilon_n = 0.08$ is included in Fig. 5, and the plot reveals that the empty lattice has a compressive strength comparable to that of the EF80 at a relative density of $\bar{\rho}$=0.09. Consequently, at a relative density of $\bar{\rho}$=0.04, which is much less than 0.09, the filled lattice has a strength which is only slightly above that of the EF80 epoxy. In contrast, at a relative density of $\bar{\rho}$=0.14 which is much above 0.09, the filled lattice has a strength which is dominated by that of the empty lattice.

4. Finite element analysis of periodic unit cells of filled and empty Kelvin lattice

4.1 Finite element formulation

Finite element (FE) simulations were performed on empty and filled Kelvin lattices using the commercial package ABAQUS/Standard[7]. The assumed constitutive laws and material data have already been summarised in Fig. 2. Recall that the grey resin is idealised as an isotropic, elastic, power law creeping solid, while the EF80 core material is taken to be a Neo-Hookean elastic solid, with $C_1 = 0.78$ and $D_1 = 0$ in the notation of ABAQUS/Standard.

The lattice is discretised using second-order tetrahedral elements (C3D10) with an element side length of $d/3$. The core (when present) is discretised using second-order tetrahedral constant-pressure elements (C3D10H) of side length on the order of $d/3$. The lattice and core (when present) share nodes at their interface. The finite element model was not taken directly from the X-ray CT scans; rather, the periodic lattice was used. Care was taken to ensure that

[7] ABAQUS/Standard version 2018 and 2020. Dassault Systèmes Simulia Corp., Providence, RI, USA.

the meshes of opposite sides of the unit cell match, so that periodic boundary conditions can be imposed in a straightforward manner on all sides of the unit cell.

4.2 Sensitivity of response to size of specimen

The finite element simulations are first used to demonstrate that the response of a periodic unit cell gives an adequate representation of the compressive response of a finite specimen. There was no need to perform simulations on the 9 x 9 x 9 finite specimen of Fig. 1(b) as it is shown in Fig. 6 that smaller specimens of 6 x 6 x 6 cells give a converged response. Finite element meshes were generated for both a periodic unit cell, as shown in Fig. 1 and for an arrangement of n x n x n unit cells, in order to idealise a finite specimen. The value of n was taken to be 1, 3 and 6 in Fig. 6.

Periodic boundary conditions were applied at the boundary of the periodic unit cell, while velocity boundary conditions were applied on the top surface of the finite specimen with the bottom surface held fixed in the z direction. For the finite size specimens, transverse displacements were either fixed at the top and bottom boundaries (sticking boundaries), to replicate the conditions of the experiments, or were free (frictionless boundaries).

Plots of nominal compressive stress σ_n versus nominal compressive strain ε_n are plotted in Fig. 6(a) for loading by frictionless platens and in Fig. 6(b) for sticking platens. The response of the periodic unit cell is added for reference. In all cases, the relative density of the empty and filled lattices is 0.09; additional simulations have been performed for a relative density of 0.04 and 0.14, and the broad conclusions given below do not change. Recall that uniaxial compression tests were performed on specimens that had integrally bonded end plates; these plates constrain the in-plane deformation of the specimen such that sticking boundary conditions are more representative that free boundary conditions.

Consider first the predictions of Fig. 6(a) for frictionless boundaries. The responses of the finite specimens range from that of the 1x1x1 unit cell specimen to that of the periodic unit cell response, for both empty and filled lattices. This is not necessarily the case for the specimens with sticking boundaries, see Fig. 6(b). The added constraints on the top and bottom boundaries, in combination with the incompressibility of the core and the dimensions of the specimens considered, imply that some specimens exhibit a stiffer response than the periodic unit cell, in particular for the filled lattices. The boundary condition of sticking grips only leads

to a slight elevation in uniaxial strength compared to frictionless boundary conditions. In broad terms, the response of the finite specimens converges rapidly with increasing size of specimen, and the periodic cell response is in excellent agreement with the finite specimen containing 6 x 6 x 6 cells.

Additional insight into the deformation mode of the filled lattice is obtained by plotting contours of core pressure in Fig. 7 for finite specimens and the periodic unit cell, at a nominal compressive strain equal to 0.1. The pressure in the core is slightly elevated in the specimens with sticking boundaries, and for both choices of boundary condition there exists a build-up in core pressure from the side face of the specimen, over the length-scale of about one unit cell. This is a boundary layer effect, and is associated with the relative deformation of core and lattice near the free boundaries: the more compliant, weaker core is able to extrude from the sides of the specimen. The size of this boundary-layer is sensitive to the ratio of strength of core to that of the lattice. In the present simulations, the contrast between the strength of the empty lattice and of the core solid is modest, and the boundary layer effect is restricted to a single layer of Kelvin cells at the sides of the specimen. A thicker boundary layer is anticipated for a weaker core. We note from Fig. 7 that for a specimen size of 3x3x3 or 6x6x6, the pressure distribution is similar to the periodic unit cell, except for a boundary layer of at most one cell.

4.3 Boundary Layer Analysis

The compressive response of an open cell lattice and incompressible core has the characteristic that the core material extrudes through the lattice and out the sides of the specimen. The relative motion of core to the lattice generates a spatial gradient in internal back-pressure of core in the vicinity of the free surface. Consequently, the core pressure inside the specimen builds up over a distance λ from almost zero at the free surface to the steady-state value associated with isochoric deformation of the filled lattice. An idealised model for this boundary layer behaviour at the side faces of the filled lattice specimen is now developed.

Idealise the lattice by a simple cubic arrangement of struts, each of length ℓ and square cross-section t x t such that the relative density is $\bar{\rho} = 3(t/\ell)^2$. Assume that yield strength of the cell-walls equals σ_w while that of the core equals σ_c. A simple shear lag calculation can be performed by imaging that cuboids of core material, of dimension λ x ℓ x ℓ, extrude out the side face when the filled lattice is compressed axially. The normal traction vanishes on the free end of the cuboid (that is, at the side-surface of the filled lattice); in contrast, the normal traction

on the other end face of the cuboid is taken to be on the order of the uniaxial compressive strength $\sigma_w \bar{\rho}^{3/2}$ of the empty lattice.

Two competing collapse mechanisms can be considered in order to obtain the dependence of shear lag length λ upon relative density and relative strength of lattice and core materials, with reference to Fig. 8. The boundary layer of extruded core materials at the sides of the specimen is shown in Fig. 8(a). At low relative density $\bar{\rho}$ the axial force on each prismatic tube F over an area of $4\lambda\ell$ of side faces of cuboid, and generated by a shear strength $\sigma_c/\sqrt{3}$ of the core, is given by $F=4\lambda\ell\sigma_c/\sqrt{3}$, see Fig. 8(b). Upon equating this force to the imbalance in axial force on the two ends of cuboid, $F=\ell^2\sigma_w\bar{\rho}^{3/2}$, we obtain

$$\frac{\lambda}{\ell} = \frac{\sqrt{3}}{4}\frac{\sigma_w}{\sigma_c}\bar{\rho}^{3/2}, \tag{2}$$

In contrast, at a high relative density, the axial force F on each prismatic tube of core of dimension λ x ℓ x ℓ is generated by the drag of lattice struts through the core, as follows. Consider the deep penetration force on a single strut of length ℓ and width t by dragging it through the core of yield strength σ_c; recall that the deep penetration pressure for pushing an indenter deep into a full space of material of strength σ_c is on the order of $6\sigma_c$. Consequently, the drag force f on this single strut is $f = 6t\ell\sigma_c$ to an adequate approximation. There exists $4\lambda/\ell$ such struts at the sides of each prismatic tube of length ℓ, but each strut is shared by two neighbouring prismatic tubes. Thus, the total drag force on each cuboid is $F = 2f\lambda/\ell = 12t\lambda\sigma_c$. Upon equating this estimate for the force F to the force imbalance $F=\ell^2\sigma_w\bar{\rho}^{3/2}$ we obtain

$$\frac{\lambda}{\ell} = \frac{\sqrt{3}}{12}\frac{\sigma_w}{\sigma_c}\bar{\rho} \tag{3}$$

The transition value of relative density at which the switch in dependence of shear lag length switches from (2) to (3) is given by $\bar{\rho} = 1/9$ such that $\lambda/\ell = 0.016\sigma_w/\sigma_c$. In the present study, we have $\sigma_w = \sigma_0$ = 34 MPa at a reference value of strain rate of $\dot{\varepsilon}_0 = 10^{-3}$ s^{-1}; also, the core strength is taken to be on the order of σ_c = 3 MPa. Consequently, the transition value of λ/ℓ is on the order of 0.2. This is consistent with the fact that the observed thickness of boundary layer in Fig. 7 does not extend beyond one unit cell size.

A more sophisticated analysis could be performed to improve the precision of the above estimate. For example, the deep penetration pressure for a punch on an elastic solid is on the

order of the Young's modulus of the solid instead of $6\sigma_c$ as assumed here for a plastic solid, see for example Gent (2001). But our intention is to give an approximate analysis to reveal the dependence of boundary layer thickness of a filled open-cell lattice upon the constituent properties of lattice and core, and upon the relative density of the lattice. The conclusion is clear: migration of the core material through the lattice is restricted to a boundary layer at the sides of the specimen. The relative flow of core through lattice is negligible when all linear dimensions of the specimen much exceed the boundary layer thickness λ.

4.4 Deformation modes of empty and filled Kelvin lattice

Before a detailed comparison can be made between the predicted and measured compressive strengths of the unfilled and filled lattices, it is instructive to first determine the effect of filling of the Kelvin lattice upon its deformation mode. A straightforward way of achieving this is to plot contours of von Mises creep strain in the cell walls of the Kelvin lattice at a fixed value of nominal macroscopic compressive strain equal to 0.2, see Fig. 9. This allows for a direct means of visualising whether the lattice deforms by a stretching mode or in an inextensional manner involving only plastic hinge formation at the nodes. The low nodal connectivity of the lattice (4 struts per node) suggests that the lattice can deform by plastic hinge formation alone in both the empty and filled states, provided the core imposes only an isochoric macroscopic constraint and does not induce local strut stretching. A sufficiently stiff and strong core will force the lattice into an affine deformation mode.

It is clear from Fig. 9 that plastic hinges exist at the nodes of the empty and filled lattices, but the precise details of the bending collapse mode changes due to the presence of the EF80 core. A small degree of stretching of horizontal struts accompanies plastic bending of the filled lattice, see the top view of Fig. 9(d). We further note from Fig. 9 that the level of accumulated plastic strain in the vicinity of the nodes in the unfilled and filled lattices is significantly above the tensile ductility on the order of 0.15 of the strut material. Consequently, the numerical simulations support the observation that strut failure occurs in both the empty and filled lattices.

5. Discussion: comparison of simulations to measurement

The predicted compressive responses of the periodic unit cells of empty Kelvin lattice are compared with the measured responses in Fig. 3(a), and likewise for the filled Kelvin lattice in

Fig. 3(b). First, consider the response of the empty Kelvin lattice. The periodic unit cell FE predictions of the collapse response are in good agreement with experiments up to a strain of $\varepsilon_n = 0.1$, beyond which the specimens exhibit strut failure and the formation of crush bands. Second, consider the filled Kelvin lattice. Again, agreement between experiments and simulations is acceptable up to a strain of $\varepsilon_n = 0.1$; at larger strains, progressive and distributed failure occurs and the FE simulations significantly overpredict the response (Fig. 3(b)).

Carlsson et al. (2023) have recently identified the lattice contribution $\Delta\sigma(\varepsilon_n)$ to the composite strength of a filled, closed cell Kelvin lattice at any macroscopic stain ε_n by making use of the Kelvin upper bound relation, such that

$$\Delta\sigma(\varepsilon_n) = \sigma_n\ (\varepsilon_n) - (1-\bar{\rho})\sigma_c(\varepsilon_n) \qquad (4)$$

where $\sigma_n(\varepsilon_n)$ is the strength of the filled lattice and $\sigma_c(\varepsilon_n)$ is the strength of the core material alone. We follow this strategy, and compare the predicted and measured lattice contributions $\Delta\sigma(\varepsilon_n)$ as a function of relative density. To do so, we first plot the measured and predicted compressive strengths of the empty lattice as $\log(\sigma_n)$ versus $\log(\bar{\rho})$ at $\varepsilon_n = 0.01$ and $\varepsilon_n = 0.08$, see Fig. 10(a). Then, we determine the lattice contribution in the form of a plot of $\log(\Delta\sigma)$ versus $\log(\bar{\rho})$, again at $\varepsilon_n = 0.01$ and $\varepsilon_n = 0.08$, see Fig. 10(b).

First consider the empty lattice; there is excellent agreement between the predicted and observed responses. At a small strain $\varepsilon_n = 0.01$, the deformation is elastic and the slope of $\log(\sigma_n)$ versus $\log(\bar{\rho})$ equals 2. Recall that a slope of 2 is expected for elastic bending of a lattice of low nodal connectivity (Gibson and Ashby, 1997). The empty lattice exceeds yield at $\varepsilon_n = 0.08$ and the slope of $\log(\sigma_n)$ versus $\log(\bar{\rho})$ drops slightly to 1.9. For a slender structure deforming in bending, we would expect the slope to be 3/2. The relative density of the Kelvin lattice is sufficiently high for the struts not to behave as slender beams and consequently the slope is expected to be higher than the classical solutions for a slender structure (Gibson and Ashby, 1997).

Next, consider the filled lattice; again, there is excellent agreement between prediction and measurement. At a small strain $\varepsilon_n = 0.01$, the contribution from the core is negligible, and the slope of $\log(\Delta\sigma)$ versus $\log(\bar{\rho})$ equal to 2 indicates a bending mode of deformation. This slope decreases to 1.6 at $\varepsilon_n = 0.08$, which is slightly below the slope for the empty lattice but is sufficiently above unity to imply that the deformation of the lattice remains bending dominated.

6. Concluding remarks

The sensitivity of the macroscopic compressive response of an open-cell Kelvin lattice to the presence of an almost incompressible core is explored in the present study. It is demonstrated both experimentally and theoretically that the presence of the core has a minor effect upon the initial elasto-plastic deformation mode of the lattice, but prevents softening and the formation of crush bands. Distributed vertical microcracking of both lattice and core occurs during a compression test on the filled lattice, thereby degrading the tangent modulus compared to that of the current elasto-plastic finite element predictions. More sophisticated constitutive models that make use of damage mechanics or cohesive zone models are required in order to describe this softening mode.

The EF80 epoxy core of the present study is sufficiently compliant and weak compared to the compressive strength of the empty lattice to have a minor effect upon the deformation mode of the filled lattice. A switch in the response of the lattice struts from bending to a much stronger mode of stretching-dominated behaviour only occurs when the uniaxial strength of the core much exceeds the compressive strength of the empty lattice.

Acknowledgements

The authors acknowledge financial support from the European Research Council in the form of an Advanced Grant (MULTILAT, 669764). JC is supported by the Gull & Stellan Ljungberg foundation. AK is supported by the Jardine Scholarship from Jardine Foundation. AS is supported by the Ashby Postdoctoral Research Fellowship from the Department of Engineering, University of Cambridge.

Appendix A. An assessment of scatter in response

A.1 The role of Plateau borders

The Kelvin lattices were manufactured with small Plateau borders present, of root radius R=0.1mm, and a strut diameter of d=0.55mm, see Fig. A1. Finite element simulations were performed in order to assess the effect of the Plateau borders upon the compressive response of both empty and filled lattices, see Fig. A1 for the choices $R/d = 0,\ 0.18$ and 0.36,

corresponding to R=0, 0.1mm and 0.2mm. The collapse response is almost insensitive to the choice of R/d.

A.2 Tensile tests on cured strut resin

The sensitivity of tensile response to the print direction of the dogbone-shaped tensile specimens has been explored as follows. Dogbone tensile specimens were manufactured by SLA, with the print direction aligned with the axial loading direction of the specimen, transverse to the loading direction and at 45^o to the loading direction. These three print directions are characteristic of the three sets of strut direction in the Kelvin lattice. For example, the inclined struts of the Kelvin lattice are printed at 45^o to the axis of the inclined strut.

Tensile tests were performed on each orientation and at strain rates of 10^{-2} s^{-1}, 10^{-3} s^{-1} and 10^{-4} s^{-1}, see Fig. A2. The degree of scatter was assessed by performing 3 nominally identical tests for each orientation and strain rate. Recall that a single test result for the 45^o orientation and 3 strain rates has already been shown in Fig. 2. The responses in Fig. A2 reveal minor scatter in stress versus strain characteristic but with greater scatter in failure strain. This is consistent with the findings of Saini et al (2020) that for 3D SLA, the scatter in tensile strength is small but the failure strain is sensitive to print direction.

A.3 Scatter in the observed compressive response of empty and filled lattices

Three repeat tests have been performed for the empty and filled lattices, at a nominal strain rate of 10^{-3} s^{-1}. The scatter is moderate for the empty lattice and can be traced to the variability in strut failure strain, see Fig. A3 (a). In contrast, the filled lattices behave in stable manner with progressive accumulation of distributed microcracking. Consequently, the degree of scatter is less than for the empty lattice, see Fig. A3(b).

References

Ashby, M.F., Evans, A.G., Fleck, N.A., Gibson, L.J., Hutchinson, J.W. and Wadley, H.N.G., 2000. Metal Foams: A Design Guide, June 2000, Butterworth-Heinemann. ISBN 0 7506 7219 6.

Carlsson, J., Deshpande, V.S. and Fleck, N.A., 2023. The compressive response of the filled Kelvin foam, *Eur. J. Mech. A*, 105018, doi: 10.1016/j.euromechsol.2023.105018.

Chen, Y., Das, R., Battley, M. and Xu, Z., 2018. Compressive and shear strengths of the ductile closed-cell Kelvin and Weaire-Phelan foams along the lattice direction [100], *Thin-walled structures* **132**, 237-249.

Comley, K. and Fleck, N. A. (2010). A micromechanical model for the Young's modulus of adipose tissue. *Int.J.Solids and Structures*, **47**, 2982-2990.

D'Mello, R.J. and Waas, A.M., 2012. Synergistic energy absorption in the axial crush response of filled circular cell honeycombs. *Compos. Struct.* **94**, 1669–1676.

D'Mello, R.J. and Waas, A.M., 2013. Inplane crush response and energy absorption of circular cell honeycomb filled with elastomer. *Compos. Struct.* **106**, 491-501.

Gent, A. N. (2001). Editor of Engineering with Rubber: how to design rubber components, 2nd edn., Hanser Publishers, Munich, ISBN 3-446-21403-8.

Gibson, L. J. and Ashby, M. F., 1997. Cellular solids. Structure and properties – second edition. Cambridge University Press.

Gong, L. Kyriakides, S. and Triantafyllidis, N., 2005. On the stability of Kelvin cell foams under compressive loads. J. Mech. Phys. Solids, **53**(4), 771-794.

Jang, W.-Y., Kyriakides, S. and Kraynik, A.M., 2010. On the compressive strength of open-cell metal foams with Kelvin and random cell structures, *Int. J. Solids Structs* **47**, 2872-2883.

Jang, W.-Y. and Kyriakides, S., 2009a. On the crushing of aluminum open-cell foams: Part I experiments, *Int. J. Solids Structs* **46**(2-3), 617-634.

Jang, W.-Y. and Kyriakides, S., 2009b. On the crushing of aluminum open-cell foams: Part II analysis, *Int. J. Solids Structs* **46**(2-3), 635-650.

Lord Kelvin (Sir William Thomson), 1887. On the Division of Space with Minimum Partitional Area, *Philosophical Magazine*, **24**(151): 503, doi:10.1080/14786448708628135.

Kwang-Min Park, Gil-Oh Kim, Jung-Gil Kim & Young-sook Roh (2022) Mechanical properties of additive manufactured variable-density Kelvin lattice structures: a novel design method for Kelvin unit cells, Journal of Structural Integrity and Maintenance, 7:1, 34-45, DOI: 10.1080/24705314.2021.1971893.

McShane, G.J., Deshpande, V.S. and Fleck N.A. (2006). The underwater blast resistance of metallic sandwich beams with prismatic lattice cores. *J. Appl. Mech*., **74**(2), 352-364.

Saini, J. S., Dowling, L., Kennedy, J., & Trimble, D. (2020). Investigations of the mechanical properties on different print orientations in SLA 3D printed resin. *Proceedings of the Institution of Mechanical Engineers, Part C: Journal of Mechanical Engineering Science*, *234*(11), 2279-2293.

Shalchy, F., Carlsson, C., Deshpande, V. and Fleck, N., 2022. Pinching of gel-filled honeycomb, *Int. J. Solids Struct.* 257(111728).

Simone, A. E. and Gibson, L. J., 1998. Effects of solid distribution on the stiffness and strength of metallic foams, *Acta mater.* **46**(6), 2139-2150.

Tagarielli, V.L., Deshpande, V.S. and Fleck, N.A. (2007). The dynamic response of composite sandwich beams to transverse impact. *Int. J. Solids Structs*., **44**, 2442-2457.

Tankasala, H., Deshpande, V. and Fleck, N., 2021. The in-plane elastic-plastic response of an incompressible, filled hexagonal honeycomb, *J. Mech. Phys. Solids* **155**, 104536.

Tvergaard, V. and Needleman, A. (1980). On the localisation of buckling patterns. *J. Applied Mech*., **47**, 613-619.

Tzortzinis, G., Gross, A. and Gerasimidis, S., 2022. Auxetic boosting of confinement in mortar by 3D reentrant truss lattices for next generation steel reinforced concrete members. *Extreme Mechanics Letters*, *52*, p.101681.

Wang, E., Chen. C., Zhang, G., Luo, Q., Li, Q. and Sun, G. 2023. Multiaxial mechanical characterization of additively manufactured open-cell Kelvin foams. *Compos. Struct.* **305**, 116505.

Warren, W. E. and Kraynik, A. M., 1997. Linear elastic behavior of a low-density Kelvin foam with open-cells, *J. Appl. Mech.* **64**, 787-794.

Weaire, D. and Phelan, R. (1994), A counter-example to Kelvin's conjecture on minimal surfaces, *Phil. Mag. Lett.*, **69**(2), 107–110. doi:10.1080/09500839408241577.

White, B.C., Garland, A., Alberdi, R. and Boyce, B.L., 2021. Interpenetrating lattices with enhanced mechanical functionality. *Addit. Manuf.* **38**, 101741.

Zhu, H.X., Knott, J.F. and Mills, N.J., 1997a. Analysis of the elastic properties of open-cell foams with tetrakaidecahedral cells. *J. Mech. Phys. Solids* **45** (3), 319-343.

Zhu, H.X., Mills, N.J. and Knott, J.F., 1997b. Analysis of the high-strain compression of open-cell foams. *J. Mech. Phys. Solids* **45** (11-12), 1875-1904.

Figure Captions

Fig. 1. Open-cell Kelvin lattices. (a) Unit cell of open-cell regular Kelvin lattice; (b) Specimen geometry.

Fig 2. (a) Tensile and compressive nominal stress versus nominal strain response of EF80 flexible epoxy; (b) tensile nominal stress versus nominal strain response of Grey V4 Resin.

Fig. 3. Compressive nominal stress versus nominal strain response of (a) empty and (b) filled Kelvin lattice. Experimental (Exp.) results are obtained using finite specimens and finite element (FE) predictions are obtained for periodic unit cells.

Fig. 4 (a) X-ray CT tomographs of a vertical slice of a compression tests on a filled lattice of relative density 0.09, and a strain rate of 10^{-3} s^{-1}; (b) sketch of crack evolution in the struts and core of the filled lattice.

Fig. 5. Nominal stress σ_n versus relative density $\bar{\rho}$ for empty and filled Kelvin lattice at nominal strain ε_n = 0.08 (near the peak for the empty lattices and just after the knee in the stress versus strain response of the filled lattice). Experimental data is shown by data points, while finite element simulations are given by solid lines.

Fig. 6. Compressive response of empty and filled specimens of different size with (a) top and bottom boundaries free in transverse direction (frictionless boundary condition) and (b) top and bottom boundaries constrained in transverse direction (sticking boundary condition). The response of a periodic unit cell is included in both (a) and (b).

Fig. 7. Contours of core pressure at compressive strain $|\varepsilon_n| = 0.1$ in periodic unit cell and in finite specimens comprising 1x1x1, 3x3x3 and 6x6x6 unit cells, with frictionless top and bottom boundaries and with sticking top and bottom boundaries.

Fig. 8 (a) Representative boundary layers at two sides of the finite specimen where side leakage occurs with respect to the lattice; (b) leakage mechanism that gives rise to a shear traction on the faces of each cuboid of core material, of dimension λ x ℓ x ℓ; (c) leakage mechanism that gives rise to a deep penetration force *f* on each strut within the boundary layer.

Fig. 9. Equivalent (von Mises) creep strain of Kelvin lattice of relative density $\bar{\rho} = 0.09$ at strain $\varepsilon_n = 0.2$: (a, c) empty and (b, d) filled. Side views are given in (a-b) and top views in (c-d).

Fig. 10. (a) σ_n versus $\bar{\rho}$ for empty lattice; (b) $\Delta\sigma/\sigma_0$ versus $\bar{\rho}$ for filled lattice. Results are shown for two choices of strain ε_n. Finite element predictions are represented by lines and experimental data by points.

Fig. A1. (a) Close-up of the unit cell showing root radius *R* and strut diameter *d*. (b) Compressive response of periodic unit cells with a root radius of *R/d* = 0, 0.18 and 0.36 for the case of $\bar{\rho} = 0.09$.

Fig. A2. Grey V4 Resin, additional data. (a-c) Tensile nominal stress versus tensile nominal strain dependence on build direction; (d) Strain rate sensitivity for the case when build direction is normal to the axial direction of the dog bone specimen; (e) Schematic of the dogbone specimen.

Fig. A3. Compressive nominal stress versus nominal strain response showing experimental scatter for (a) empty and (b) filled Kelvin lattice for three choices of relative density $\bar{\rho}$, and a nominal strain rate of 10^{-3} s^{-1}.

Figures

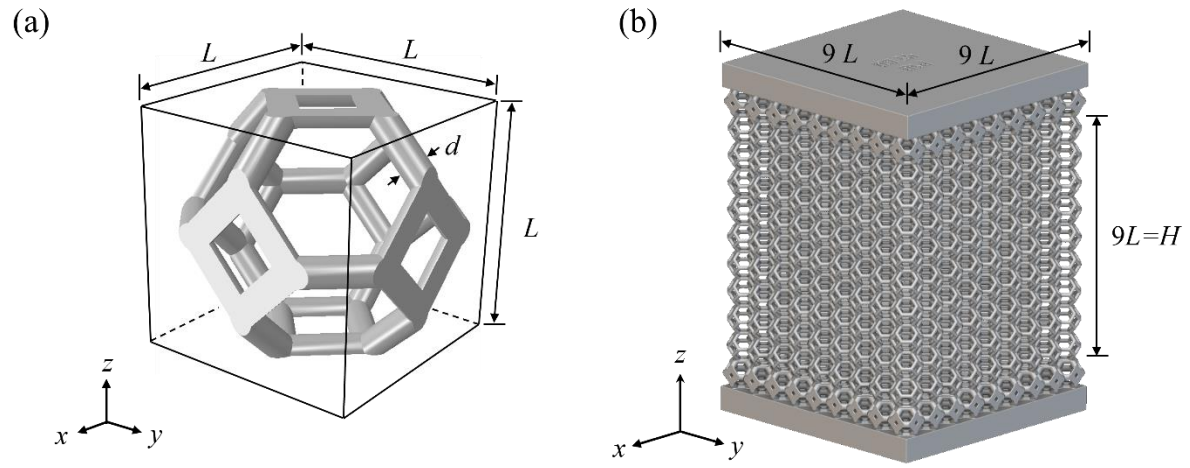

Fig. 1. Open-cell Kelvin lattices. (a) Unit cell of open-cell regular Kelvin lattice; (b) Specimen geometry.

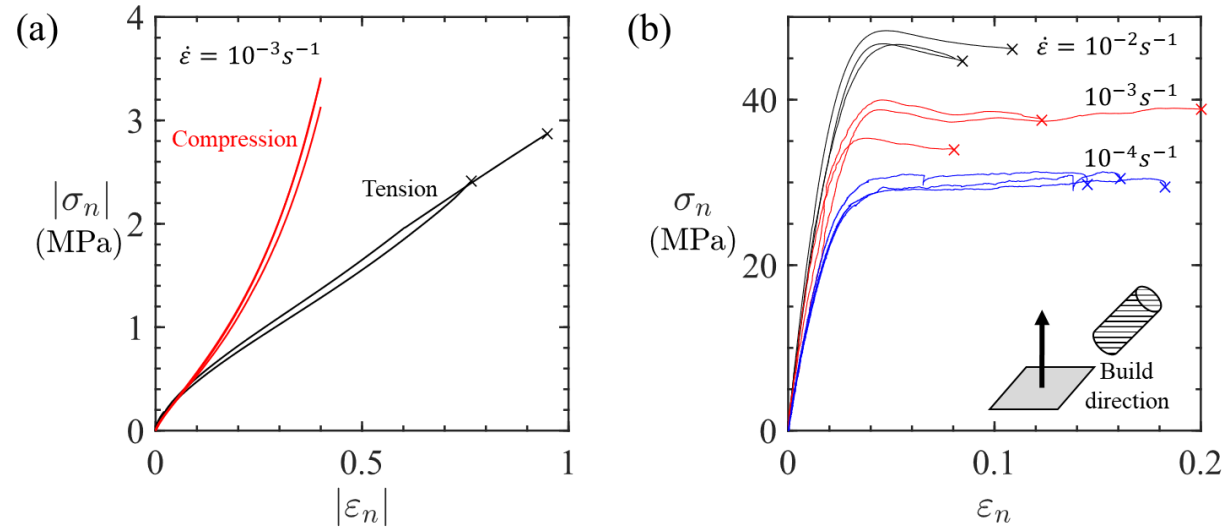

Fig 2. (a) Tensile and compressive nominal stress versus nominal strain response of EF80 flexible epoxy; (b) tensile nominal stress versus nominal strain response of Grey V4 Resin.

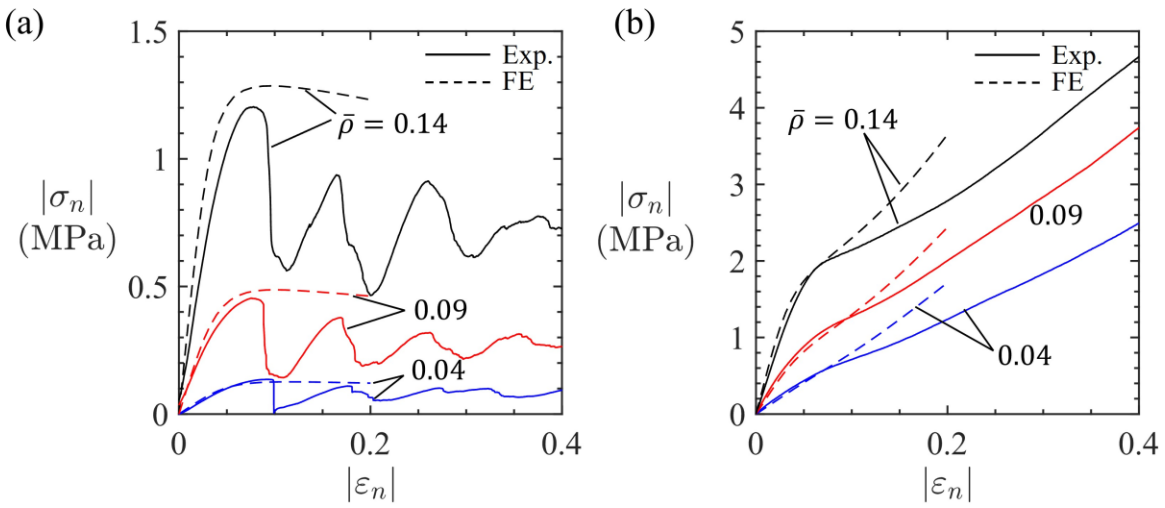

Fig. 3. Compressive nominal stress versus nominal strain response of (a) empty and (b) filled Kelvin lattice. Experimental (Exp.) results are obtained using finite specimens and finite element (FE) predictions are obtained for periodic unit cells.

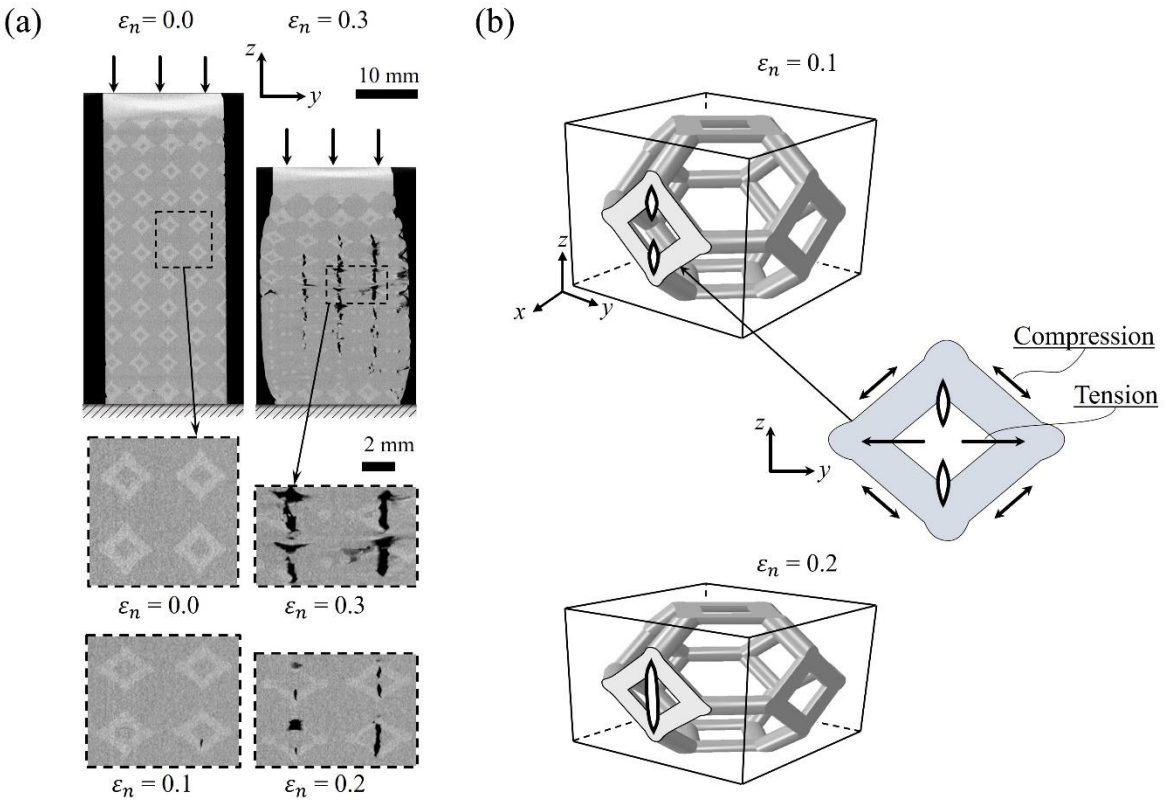

Fig. 4 (a) X-ray CT tomographs of a vertical slice of a compression tests on a filled lattice of relative density 0.09, and a strain rate of 10^{-3} s^{-1}; (b) sketch of crack evolution in the struts and core of the filled lattice.

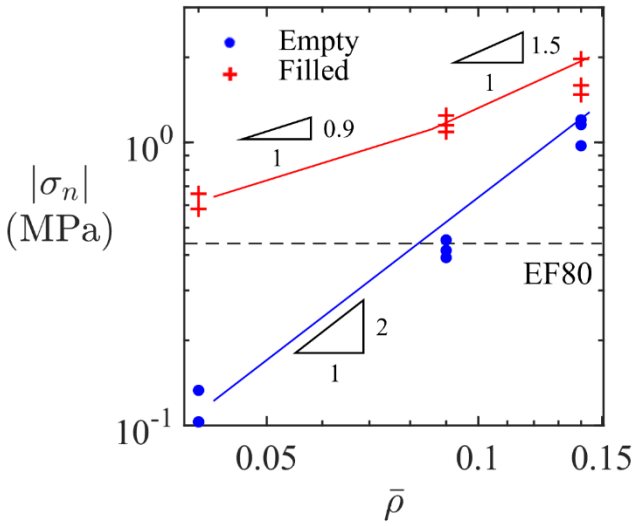

Fig. 5. Nominal stress σ_n versus relative density $\bar{\rho}$ for empty and filled Kelvin lattice at nominal strain ε_n = 0.08 (near the peak for the empty lattices and just after the knee in the stress versus strain response of the filled lattice). Experimental data is shown by data points, while finite element simulations are given by solid lines.

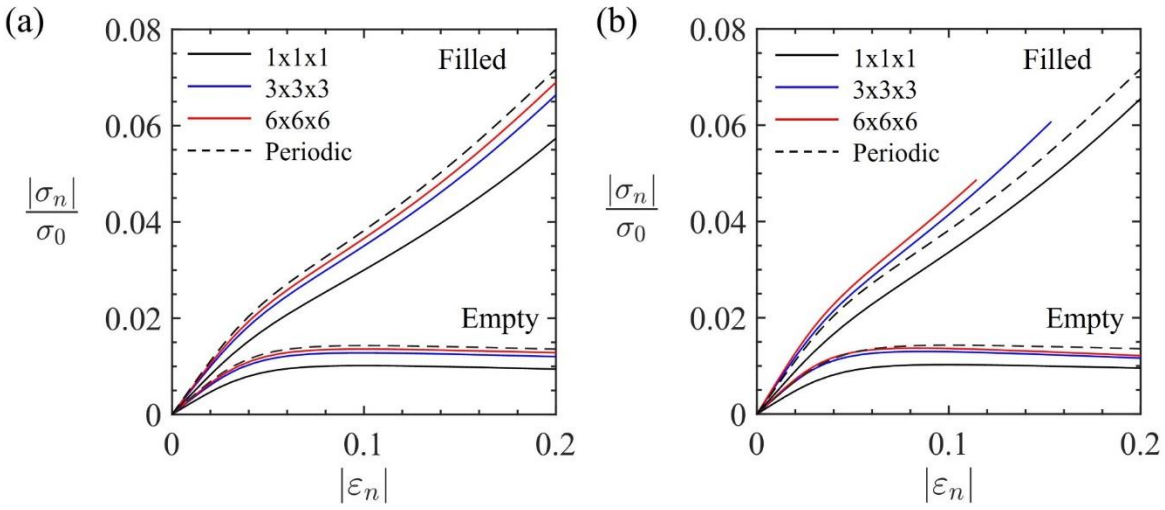

Fig. 6. Compressive response of empty and filled specimens of different size with (a) top and bottom boundaries free in transverse direction (frictionless boundary condition) and (b) top and bottom boundaries constrained in transverse direction (sticking boundary condition). The response of a periodic unit cell is included in both (a) and (b).

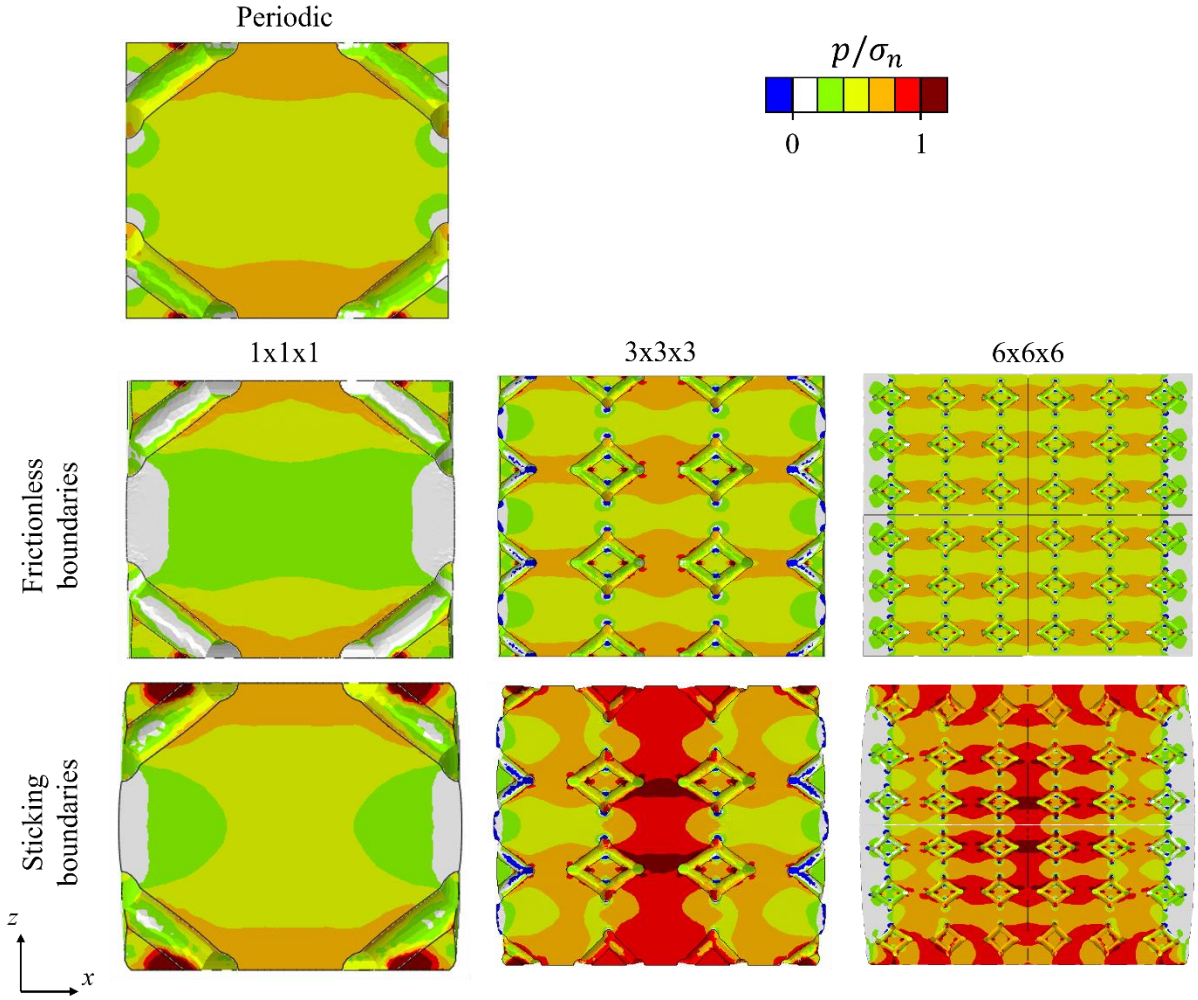

Fig. 7. Contours of core pressure at compressive strain $|\varepsilon_n| = 0.1$ in periodic unit cell and in finite specimens comprising 1x1x1, 3x3x3 and 6x6x6 unit cells, with frictionless top and bottom boundaries and with sticking top and bottom boundaries.

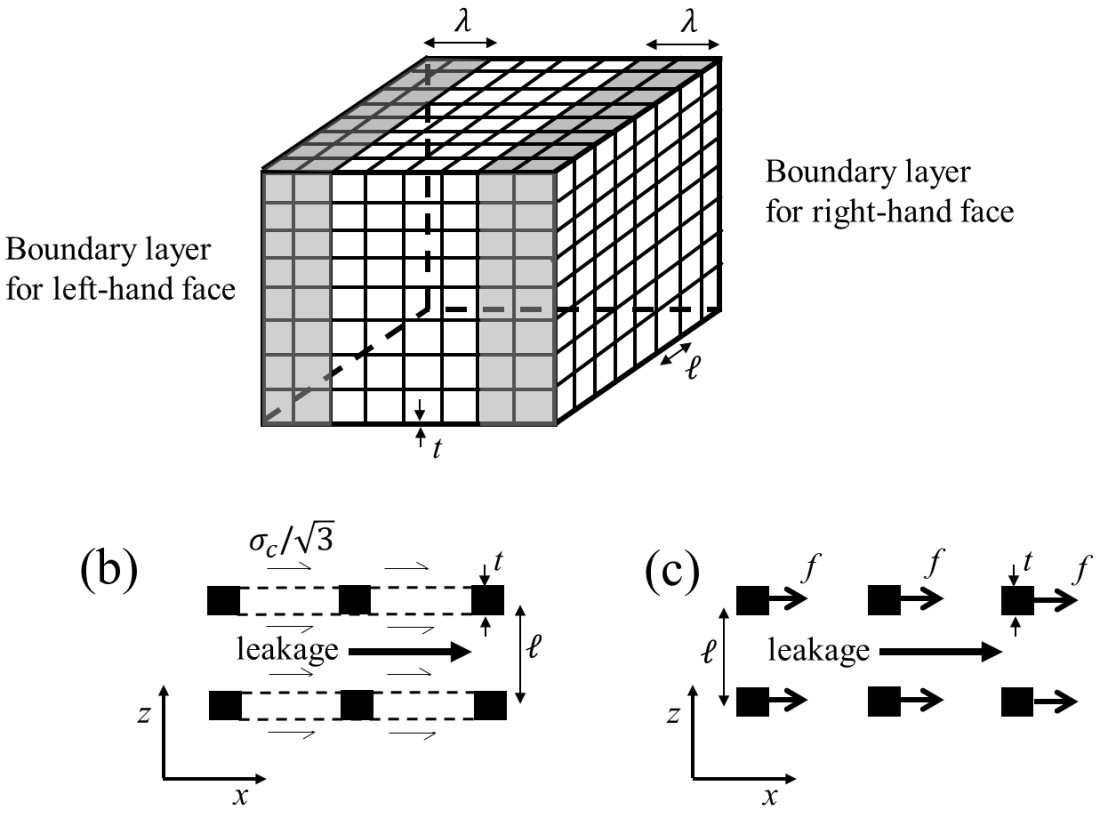

Fig. 8 (a) Representative boundary layers at two sides of the finite specimen where side leakage occurs with respect to the lattice; (b) leakage mechanism that gives rise to a shear traction on the faces of each cuboid of core material, of dimension λ x ℓ x ℓ; (c) leakage mechanism that gives rise to a deep penetration force f on each strut within the boundary layer.

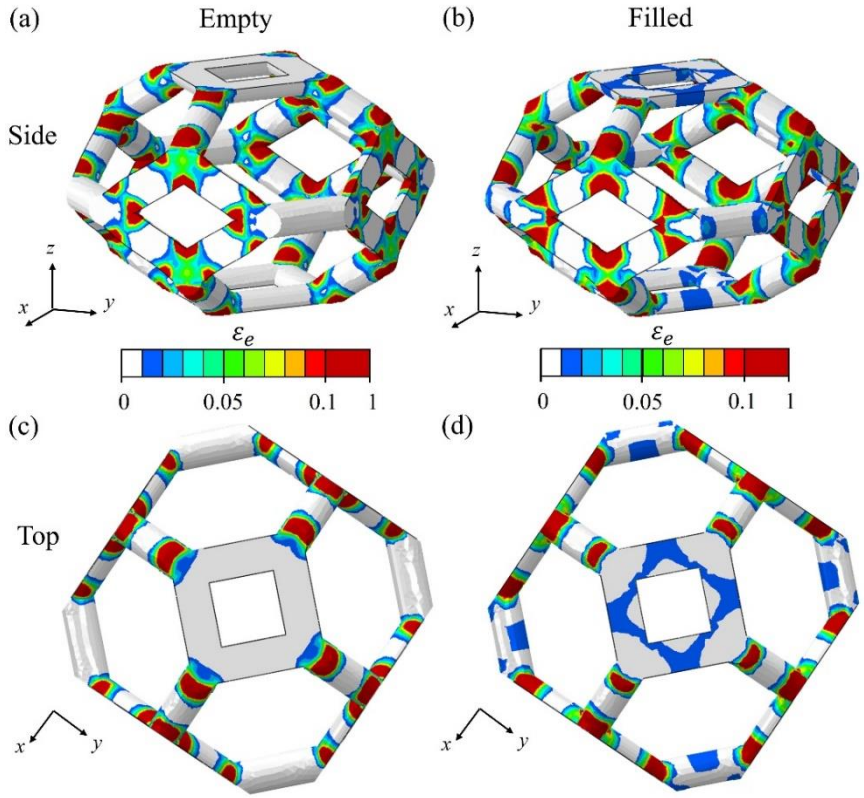

Fig. 9. Equivalent (von Mises) creep strain of Kelvin lattice of relative density $\bar{\rho} = 0.09$ at strain $\varepsilon_n = 0.2$: (a, c) empty and (b, d) filled. Side views are given in (a-b) and top views in (c-d).

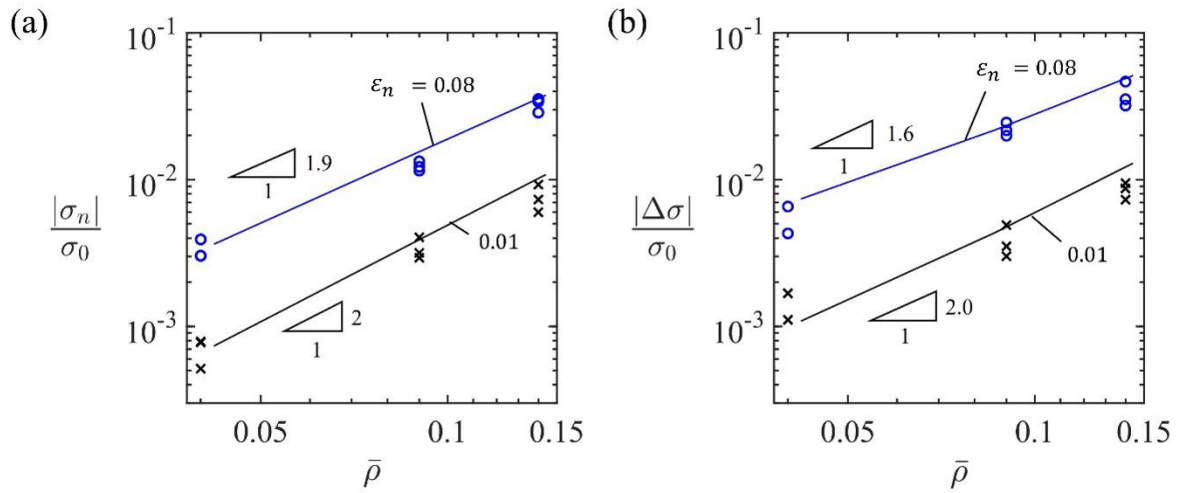

Fig. 10. (a) σ_n versus $\bar{\rho}$ for empty lattice; (b) $\Delta\sigma/\sigma_0$ versus $\bar{\rho}$ for filled lattice. Results are shown for two choices of strain ε_n. Finite element predictions are represented by lines and experimental data by points.

Appendix Figures

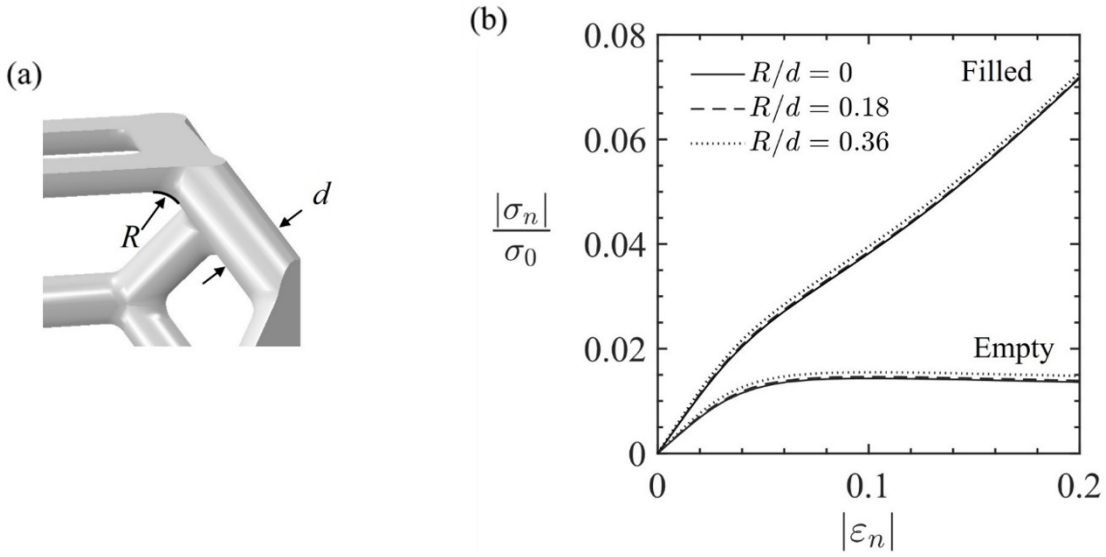

Fig. A1. (a) Close-up of the unit cell showing root radius *R* and strut diameter *d*; (b) Compressive response of periodic unit cells with a root radius of *R/d* = 0, 0.18 and 0.36 for the case of $\bar{\rho} = 0.09$.

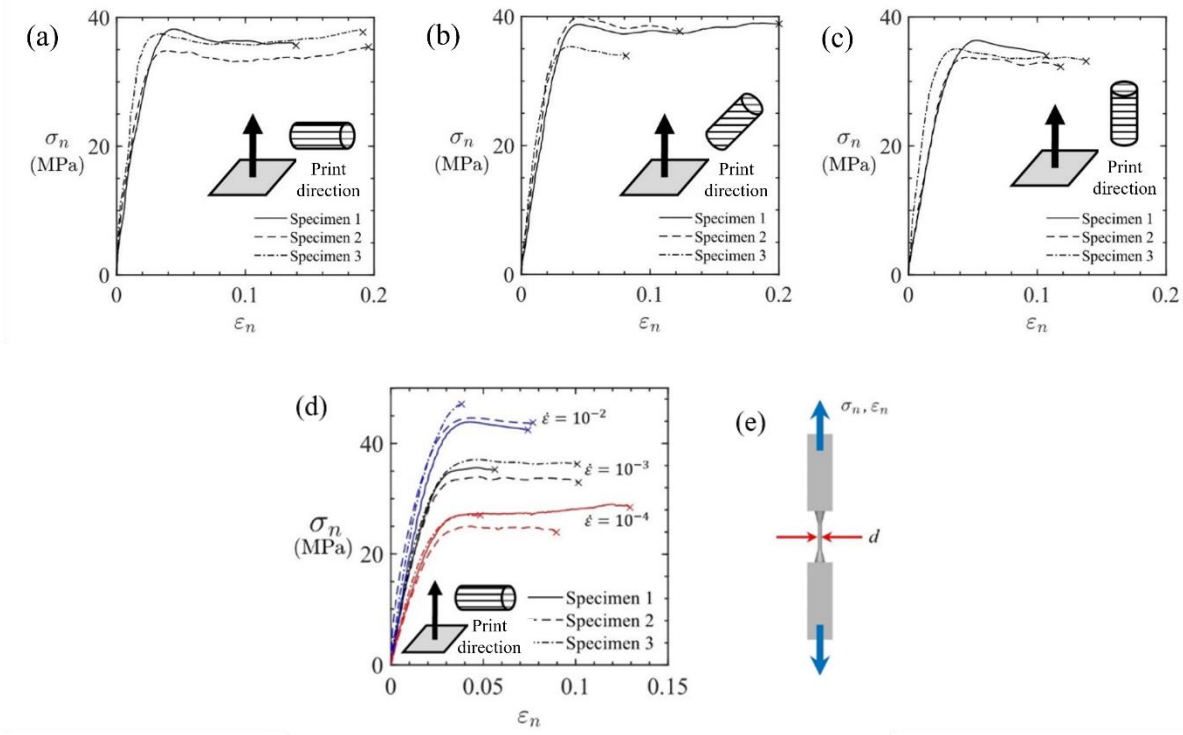

Fig. A2. Grey V4 Resin, additional data. (a-c) Tensile nominal stress versus tensile nominal strain dependence on build direction; (d) Strain rate sensitivity for the case when build direction is normal to the axial direction of the dog bone specimen; (e) Schematic of the dogbone specimen.

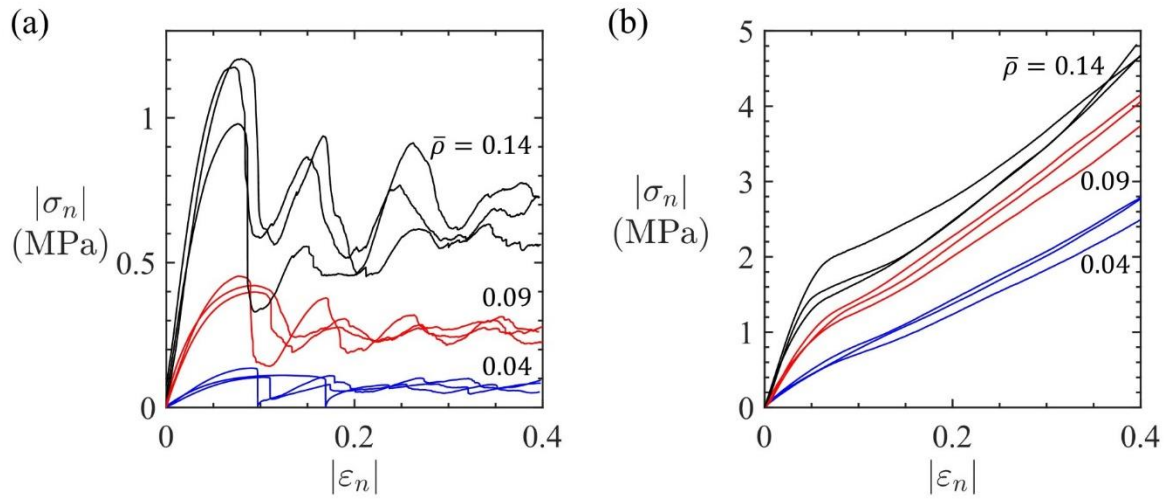

Fig. A3. Compressive nominal stress versus nominal strain response showing experimental scatter for (a) empty and (b) filled Kelvin lattice for three choices of relative density $\bar{\rho}$, and a nominal strain rate of 10^{-3} s^{-1}.